EXPERIMENTAL AND NUMERICAL INVESTIGATION OF THE ISO-THERMAL FLOW FIELD IN A NOVEL SOLAR EXPANDING-VORTEX PARTICLE REACTOR

Alfonso CHINNICI[1, 2*], Maziar ARJOMANDI[1, 2], Zhao LU[1, 2], Zhao Feng TIAN[1, 2] and Graham J. NATHAN[1, 2]

[1] School of Mechanical Engineering, the University of Adelaide, Australia.

[2] Centre of Energy Technologies, the University of Adelaide, Australia
*Corresponding author, E-mail address: alfonso.chinnici@adelaide.edu.au

ABSTRACT

The present study reports an experimental and numerical investigation of the iso-thermal flow field in a novel concept of Solar Vortex Reactor, termed the Solar Expanding-Vortex Particle Reactor, SEVR. This configuration differs from the previous reactor configurations by features including utilizing a conical entry at the opposite end of the cavity to the aperture and a radial exit. Three-dimensional velocity components were measured at different locations, revealing a complex flow field within the device. The effect of changing the reactor geometric features on the vortex structure is also analysed. A three-dimensional Computational Fluid Dynamics (CFD) model of the SEVR was developed. Three two-equation turbulence models, namely standard k-ε model, Re-Normalisation Group (RNG) k-ε model with swirl factor, and k-ω Shear Stress Transport (SST) models were used to simulate the flow field within the SEVR. The validity of the CFD model was assessed by comparison with the collected experimental data for the fluid phase. It has been found that the predictions of the RNG k-ε model with swirl factor are in reasonable agreement with the experimental data while the standard k-ε model fails in predicting the main characteristics of the observed vortex structure.

INTRODUCTION

The use of directly-irradiated particle receivers for Concentrated Solar Thermal (CST) technology has received growing attention due to their potential to achieve higher temperatures and higher efficiency than is possible with tubular receivers (Ho and Iverson, 2014). One of the most promising directly irradiated solar reactor is the Solar Vortex Reactor, SVR, which has been found to have a relatively high energy conversion efficiency among several directly irradiated solar reactors and it has been applied successfully to several applications, e.g. gasification of carbonaceous materials (Steinfeld, 2005; Z'Graggen, 2008; Piatkowski and Steinfeld, 2011). The SVR consists of a transparent window, a secondary concentrator (SC), an aperture and a cylindrical cavity. Fluid substances and solid particles are injected tangentially into the SVR to generate a vortex flow within it. The tangentially injected fluid transports the particles through the reactor, resulting in an efficient absorption of the concentrated solar radiation and mixing. However, despite its advantages, the original configuration of SVR has one major limitation that poses a great challenge to the continuous operation of this reactor, namely the propensity to deposit particles onto the reactor window (Steinfeld, 2005; Ozalp et al., 2013).

Several works (Kogan and Kogan 2002; Hirsch and Steinfeld 2004; Steinfeld et al., 1998; Shilapuram et al. 2011; Kogan et al., 2004; Kogan et al., 2007) have shown that the vortex structure within the SVR strongly affects the particle deposition onto the reactor window. However, only limited relevant experimental measurements of the flow field within the SVR (Meier et al, 1996; Ozalp et al., 2013) and qualitative analysis of the particle deposition on the receiver window are available in literature, so that the mechanisms which control the propensity of the particles to deposit onto the receiver window are still poorly understood. Current SVR designs adopt auxiliary gas jets to form a curtain of shielding gases to mitigate particle deposition. However, this solution is not very effective, with the purging gas nozzle locations strongly dependent on the fluid-dynamic flow structure established in the cavity and the operating conditions adopted (Tian et al., 2015). Hence, there is a need to optimise the fluid-dynamic structure of the vortex within the SVG to prevent particles from depositing onto the reactor window without the use of shielding gas flow.

Recently, the Centre of Energy Technology in the University of Adelaide proposed a novel concept of SVR, termed the Solar Expanding-Vortex Particle Reactor SEVR, together with the aerodynamic mechanism that offers potential to greatly mitigate the problem of particle deposition onto the window (Chinnici et al., 2015). This mechanism has been identified by a systematic investigation of the effect of receiver geometry on the vortex structure using a Computational Fluid Dynamics (CFD) model validated against the experimental data for the existing configuration of SVR (Z'Graggen et al., 2006; Ozalp et al., 2013). However, the model is yet to be validated for the new SEVR configurations, so that experimental data are required to confirm and/or refine the CFD study. For this reason, the present paper reports the experimental and numerical analysis of the iso-thermal flow field within the patented SEVR. The overall objective of this study is to characterize the vortex structure within the SEVR and to provide a set of experimental data of the gas-particle flow in the SEVR for CFD model validation.

SOLAR EXPANDING-VORTEX REACTOR CONFIGURATION

The SEVR is shown schematically in Figure 1. Its design has been previously described in detail (Chinnici et al., 2015); only the main features are highlighted here.

Figure 1a) also reports the location where the measurement of flow characteristics was conducted. The SVER configuration (its body was made of stainless steel) differs from the previously reported SVR configurations (Z'Graggen et al., 2006; 2008; Hirsch and Steinfeld 2004)
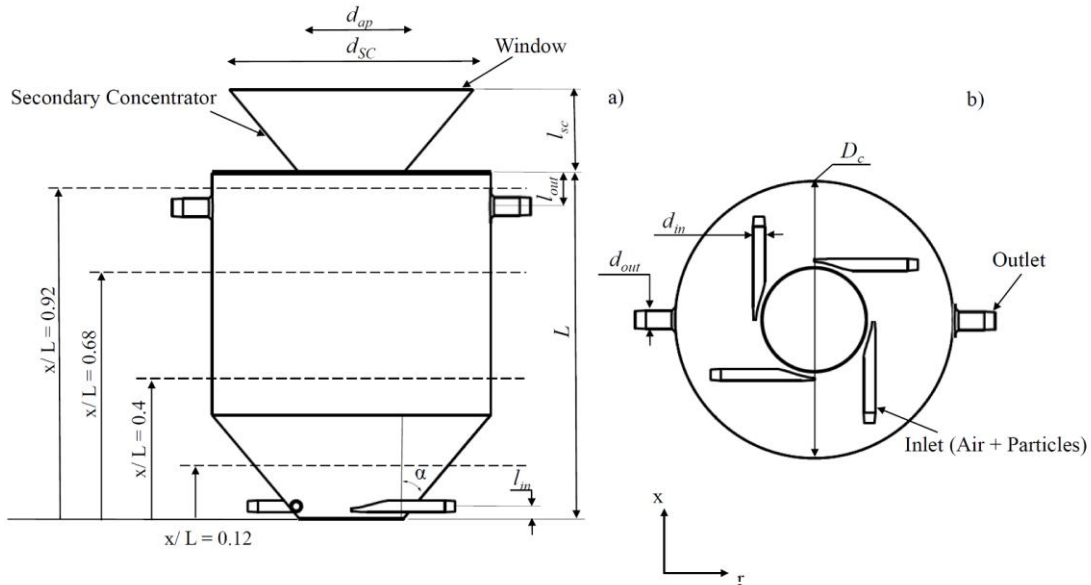

Figure 1: Schematic diagram of the Solar Expanding-Vortex Reactor, showing (a) a side view and (b) a bottom view. Figure 1 a) also reports the exact locations of the flow measurement.

by using a conical entry at the opposite end of the cavity to the aperture and radial exits on the upper part of the cylindrical section. With this arrangement the vortex intensity at the plane of the aperture has reduced substantially relative to the vortex intensity at the inlet plane of the flow, in contrast to the SVR (Chinnici et al., 2015). Nevertheless, like the SVR, the aperture is closed by a transparent window, it uses a secondary concentrator (SC) and employs tangential inlets to generate a vortex flow that transport the fluid substances and solid particles into the cavity. The SC (made of acrylic) chosen for the present analysis is cylindrical (although a typical conical shape is reported in Figure 1) to provide further optical access. However, the shape of the SC can be expected to have only a secondary influence on the flow within the chamber, so that assessing its influence is beyond the scope of the present investigation. For all the configurations analysed, the reactor orientation was vertical. This orientation requires a beam-down configuration, i.e. the tower-mounted reactor is aligned with the axis of the heliostat field, with the need of an additional reflective surface (Segal and Epstein, 2003). For the present assessment, a pilot scale reactor was chosen with a solar input of 100 kW. The geometrical details of the SEVR configuration investigated in the present study and the nomenclature used on Fig. 1 are reported in Table 1.

Parameter	Value
L, mm	500
D_c, mm	400
α, °	50
d_{ap}, mm	50-100-150-200
d_{in}, mm	12.5
d_{out}, mm	21
d_{SC}, mm	200
l_{SC}, mm	125

Table 1: Geometrical details of the SEVR configurations investigated in the present study.

EXPERIMENTAL AND NUMERICAL PROCEDURE

In the single-phase experiment air at 298 K was injected into the cavity through the four tangential inlets. The jets were generated by a compressed air source, delivered through a long, round pipe to ensure fully developed flow conditions before the reactor inlets. The total inlet volumetric flow rate, Q, was 14 *L/s*. A Turbulent Flow Instrumentation brand Cobra probe was used to obtain three-dimensional velocity components (with an accuracy of ± 0.3 m/s within ± 45° of the probe x-axis) at different cross-sections through the SEVR. The probe is a multi-hole pressure probe that provides dynamic, three-dimensional velocity components and local pressure measurements in real-time. It was mounted on a manual traverse horizontally with a positioning accuracy of 0.01 mm in the radial direction. By adjusting the position of the manual traverse, the cobra probe was inserted into the cavity through the holes and moved along the radial direction of the SEVR to measure the flow

properties. A sampling rate of 1.25 kHz was set on the probe and the sampling time of 6.5 s was selected (for a total of 8125 measurements). Due to limitations in its range of measurement, the cobra probe could provide accurate measurements of three-dimensional velocity components when the average flow velocity was between 2 m/s and 50 m/s. For the operative conditions adopted in this study, the average flow velocity in the inner region of the SEVR was below 2 m/s, so that no data was collected in this region.

A commercial CFD code, ANSYS/FLUENT 14.5 was employed for the simulations of fluid flow, turbulent species transport and particle tracking in the SEVR. The operational conditions adopted in the numerical simulations were the same of those employed in the experimental analysis. The three-dimensional geometry was built in Gambit and a non-uniform unstructured grid was generated with ANSYS/Meshing 14.5. Mesh independence and mesh quality were checked to ensure the suitability of the mesh. In particular, the mesh quality was checked for skewness (the maximum cell skewness was < 0.85), aspect ratio, orthogonality and expansion factor, accordingly to Tian et al. (2015). A total of approximately 2 million cells was employed for all configurations tested. The mesh independence was checked on a coarser mesh (1 million of cells) and a denser mesh (5 million of cells), comparing the exit velocity, location and magnitude of the maximum tangential velocity at x/L = 0.12 and at the aperture plane (the difference between the results obtained with the chosen mesh and the denser mesh was less than 5%). Three turbulence models, namely standard k-ε model, Re-Normalisation Group (RNG) k-ε model with swirl factor, and k-ω Shear Stress Transport (SST) model were used to simulate the flow field within the SEVR. Velocity inlet, pressure outlet (with zero relative gauge pressure) and wall boundary conditions were employed to define the reactor inlet, exits and walls, respectively. The effect of gravity (acting in the x-direction) was included in the simulation. The SIMPLE algorithm was employed for pressure-velocity coupling. Scalable wall function was employed for k-ε standard and RNG k-ε models, while a refined mesh with $y^+ \approx 1$ was adopted for the k-ω SST model. All the equations were discretised using the second order upwind scheme. Simulations were considered to be converged when all the residuals reached 10^{-6}. All the calculations were performed on a computer with Intel® Core™ i7 4700HQ processor and an available RAM of 16.0 GB. The CPU-time required to achieve the desired convergence varied between 14 and 18 hours.

RESULTS

Figure 2 presents the measured and calculated (with the RNG k-ε model) radial profiles of the mean tangential (absolute value) and axial velocities, normalised by the inlet velocity, U_{in}, at four cross-sections through the SEVR for $d_{ap}/D_c = 0.5$ (plane θ, r). The plane (θ, r) refers to the orthogonal plane at the reactor outlet. The exact location of the measurements is reported in Figure 1. Experimental and numerical analysis revealed key details of the flow field within the device. It can be seen that the SEVR generates a well-defined vortex flow pattern. In the lower part of the reactor (x/L = 0.12), the vortex pattern is similar to a forced vortex (Xue et al., 2011), with the maximum of tangential velocity located near the wall.

However, at x/L = 0.4 the flow undergoes a transition and in the upper part of the reactor (x/L = 0.68 and 0.92), a combined (free and forced) vortex (Xue et al., 2011) can be seen. Furthermore, it can be seen that the intensity of the vortex is inversely related to the distance from the window, due to the particular design of the SEVR. That is, it is strong at the reactor inlet, but its intensity reduces as the vortex expands through the cone. Close to the aperture plane (x/L = 0.92), the vortex intensity is reduced significantly relative to its strength at the inlet plane for the flow. From the mean axial velocity profiles, it can be seen that the axial velocity reaches its maximum near the wall, while a reversed flow is generated in the core region of the vortex. At x/L = 0.92, the axial velocity is close to zero.

Good agreement between the predictions of the RNG k-ε model with swirl factor and the measured mean tangential and axial velocity profiles was found. In particular, the model developed was able to predict the gradual transformation from a forced vortex structure to a combined structure (free and forced) along the SEVR, and the presence of a reversed flow in the core region of the vortex.

Similar numerical analysis has been performed also with the k-ε standard and k-ω SST models. To assess the validity of the models employed in this study, a validation process was undertaken by comparison of the calculated velocity profiles and the measured data. Table 2 and 3 report some of the details of the comparison process and the level of agreement that has been obtained. The latter is evaluated as the difference between the calculated and experimental data based on the magnitude of the maximum tangential velocity ($\Delta_{v,max}$) and its location along the radial direction of the reactor ($\Delta_{r,v,max}$) as well as the maximum of axial velocity ($\Delta_{u,max}$) and its location along the radial direction of the reactor ($\Delta_{r,u,max}$). In particular:

$$\Delta_{v,max} = \left| \frac{v_{max,num} - v_{max,exp}}{v_{max,exp}} \right| 100, \quad (1)$$

$$\Delta_{r,v,max} = \left| \frac{r_{v,max,num} - r_{v,max,exp}}{r_{v,max,exp}} \right| 100, \quad (2)$$

$$\Delta_{u,max} = \left| \frac{u_{max,num} - u_{max,exp}}{u_{max,exp}} \right| 100, \quad (3)$$

$$\Delta_{r,u,max} = \left| \frac{r_{u,max,num} - r_{u,max,exp}}{r_{u,max,exp}} \right| 100. \quad (4)$$

Location	Model	$\Delta_{v,max}$ %	$\Delta_{r,v,max}$ %
x/L = 0.12	k-ε standard	12.5	10.3
	RNG k-ε + swirl factor	6.2	8.5
	k-ω SST	8.5	9.2
x/L = 0.4	k-ε standard	18.5	36.3
	RNG k-ε + swirl factor	5.2	9.2
	k-ω SST	10.5	13.2
x/L = 0.68	k-ε standard	19.7	39.7
	RNG k-ε + swirl factor	5.2	9.2
	k-ω SST	12.5	11.2
x/L = 0.92	k-ε standard	20.1	38.2
	RNG k-ε + swirl factor	7.3	15.2
	k-ω SST	14.1	19.2

Table 2: Details of the validation process undertaken and level of agreement obtained. The latter is reported as the

difference between the experimental data and the models in terms of magnitude of maximum tangential velocity ($\Delta_{v,max}$), its location along the radial axis of the reactor ($\Delta_{r,v,max}$).
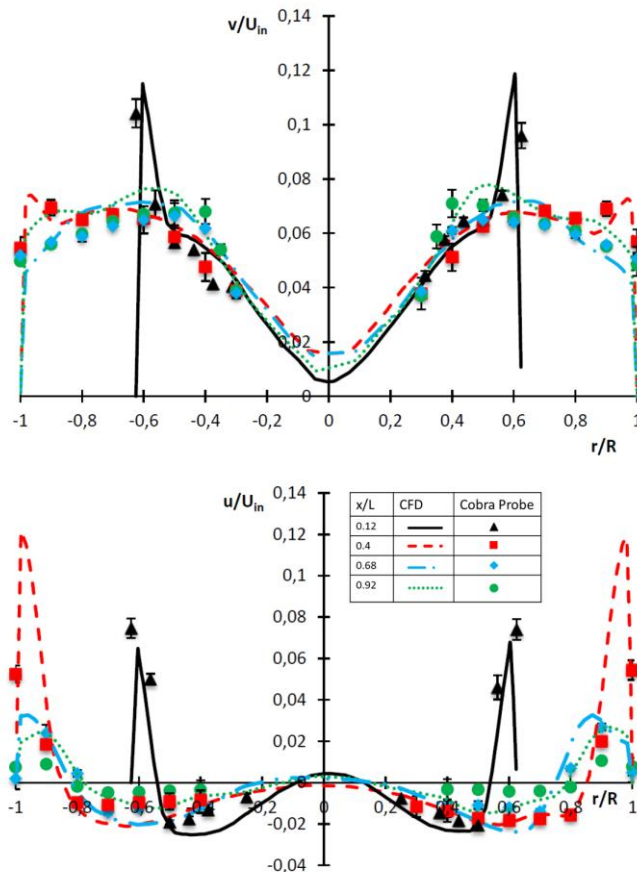
Location	Model	$\Delta_{u,max}$ %	$\Delta_{r,u,max}$ %
x/ L = 0.12	k-ε standard	5.5	6.2
	RNG k-ε + swirl factor	3.2	3.7
	k-ω SST	4.7	4.1
x/ L = 0.4	k-ε standard	44.3	10.3
	RNG k-ε + swirl factor	41.2	4.2
	k-ω SST	38.7	4.8
x/ L = 0.68	k-ε standard	9.8	14.1
	RNG k-ε + swirl factor	4.2	6.2
	k-ω SST	5.7	8.6
x/ L = 0.92	k-ε standard	10.9	12.5
	RNG k-ε + swirl factor	9.5	9.4
	k-ω SST	10.1	11.2

Table 3: Details of the validation process undertaken and level of agreement obtained. The latter is reported as difference between the experimental data and the models in terms of magnitude of maximum axial velocity ($\Delta_{u,max}$), its location along the radial axis of the reactor ($\Delta_{r,u,max}$).

Tables 2 and 3 highlight that not all the closure

data. More specifically, the use of k-ε standard model results in large discrepancies between the measured and calculated velocity profiles, predicting a forced vortex instead of a combined one in the upper part of the reactor. Such unrealistic behaviour is documented in literature (Cortes and Gil, 2007). The k-ω SST and RNG K-ε with swirl factor models show a good agreement with experimental data. In particular, of the models tested, RNG k-ε model with swirl factor shows the best agreement with the experimental data. Therefore, the RNG k-ε model with swirl factor was implemented in the current study to further investigate the influence of the geometrical parameters of the SEVR on the vortex structure.

To assess the influence of the aperture size on the vortex structure within the SEVR, a numerical analysis of the iso-thermal flow-field was performed varying d_{ap}/D_c. Figure 3 reports the comparison of the calculated mean tangential (absolute value) and axial velocity, normalised by the inlet velocity, U_{in}, at three cross-sections through the SEVR for d_{ap}/D_c = 0.125 and 0.5. It can be seen that similar tangential and axial velocity profiles were obtained along the reactor height for both values of d_{ap}/D_c investigated. This highlights that the aperture size does not significantly influence the vortex structure within the cavity. The latter is only related to the cavity geometric

models tested are in an agreement with the experimental

features. Other values of d_{ap}/D_c were investigated (d_{ap}/D_c =

Figure 2: Measured (symbols) and calculated (lines) values of tangential and axial velocity at four cross-sections through the SEVR for d_{ap}/D_c = 0.5 at the plane (θ, r). The standard deviations are given as error bars. The calculated values were obtained with the RNG k-ε model with swirl factor.

0.25 and 0.375, not shown). These cases confirmed the trend reported in Figure 3.
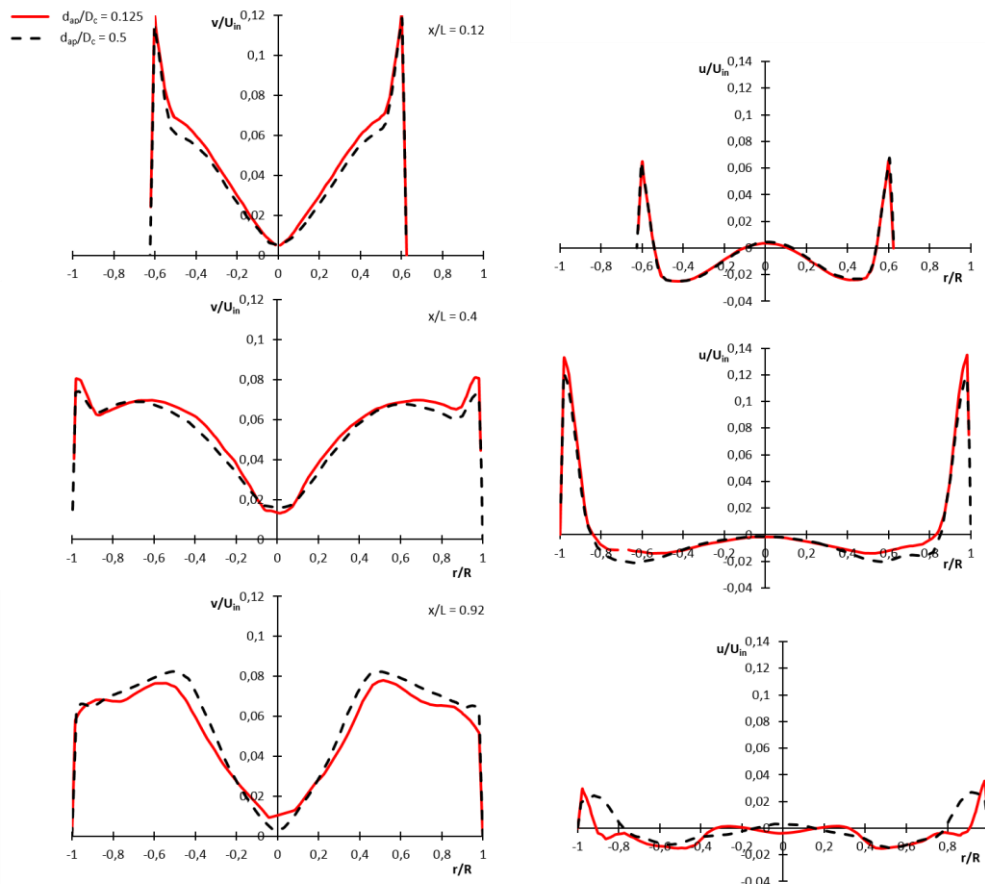

Figure 3: Calculated values of tangential and axial velocity at three cross-sections through the SEVR for $d_{ap}/D_c = 0.125$ and 0.5 at the plane (θ, r). The calculated values were obtained with the RNG k-ε model with swirl factor.

CONCLUSION

An experimental and numerical investigation of the iso-thermal flow field within a Solar Expanding-Vortex Particle Reactor was performed. Three turbulence models (RANS approach), namely k-ε standard, RNG k-ε with swirl factor, and k-ω SST were tested, by comparison of the calculated mean tangential and axial velocity within the SEVR with the collected experimental data for the fluid phase. It has been found that, of the models tested, the RNG k-ε model with a swirl factor shows the best agreement with the experimental data while the k-ε standard model fails to predict the main characteristics of the observed vortex structure. The predictions of the k-ω SST model are in reasonable agreement with the experimental data. Numerical analysis also revealed that the value of the aperture size has only a small influence on the vortex structure within the reactor cavity.

ACKNOWLEDGEMENTS

REFERENCES

CHINNICI, A., ARJOMANDI, M., TIAN, Z.F., LU, Z., NATHAN, G.J. (2015). "A novel Solar-Expanding-Vortex Flow Reactor: Influence of Vortex Structure on Particles Residence Time and trajectories", *Solar Energy,* **122**, 58-75.

CORTES, C., GIL, A. (2007) "Modeling the gas and particle flow inside cyclone separators", *Prog. Energ. Comb*, **33** (5), 409-452.

HIRSCH, D., STEINFELD, A. (2004). "Solar hydrogen production by thermal decomposition of natural gas using a vortex-flow reactor", *Int. J. of Hydrogen Energy,* **29**, 47– 55.

HO, C.K., IVERSON, B.D. (2014). "Review of high-temperature central receiver designs for concentrating solar power", *Renewable and Sustainable Energy Reviews,* **29**, 835–846.

KOGAN, A., KOGAN M. (2002). "The Tornado Flow Configuration - An Effective Method for Screening of a Solar Reactor Window", *J. of Solar Energy Engineering,* **124**(3), 206-214.

KOGAN, A. (2004). "Production of hydrogen and carbon by solar thermal methane splitting. II. Room temperature simulation tests of seeded solar reactor", *Int. J. of Hydrogen Energy,* **29**(12): 1227-1236.

KOGAN, A., ISRAELI, M., ALCOBI, E. (2007). "Production of hydrogen and carbon by solar thermal methane splitting. IV. Preliminary simulation of a confined tornado flow configuration by computational fluid dynamics", *Int. J. of Hydrogen Energy,* **32**(18): 4800-4810.

MEIER, A., GANZ, J. and STEINFELD, A. (1996) "Modeling of a novel high-temperature solar chemical

reactor", *Chemical Engineering Science*, **51** (11), 3181–3186.

OZALP, N., CHIEN, M., MORRISON, G. (2013). "Computational Fluid Dynamics and Particle Image Velocimetry Characterization of a Solar Cyclone Reactor", *J. of Solar Energy Engineering,* **135**(3), 031003.

PIATKOWSKI, N., STEINFELD, A. (2011). "Solar gasification of carbonaceous waste feedstocks in a packed-bed reactor-Dynamic modeling and experimental validation", *AIChE Journal,* **57**(12), 3522-3533.

SEGAL, A., EPSTEIN, M. (2003). "Solar Ground Reformer", *Solar Energy*, 75 (**6**), 479-490.

SHILAPURAM, V., JAYA KRISHNA, D., OZALP, N. (2011). "Residence time distribution and flow field study of aero-shielded solar cyclone reactor for emission-free generation of hydrogen", *Int. J. of Hydrogen Energy,* **36**(21), 13488-13500.

STEINFELD, A. (2005). "Solar thermochemical production of hydrogen—a review", *Solar Energy,* **78**(5), 603-615.

STEINFELD, A., BRACK, M., MEIER, A., WEIDENKAFF, A., WUILLEMIN, D. (1998). "A Solar Chemical Reactor for Co-production of Zinc and Synthesis gas", *Energy,* **23**(30), 803-814.

XUE, Y., ARJOMANDI, M., KELSO, R. (2011) "Visualization of the flow structure in a vortex tube", *Experimental Thermal and Fluid Science*, **35**(8), 1514-1521.

Z'GRAGGEN, A., HAUETER, P., TROMMER, D., ROMERO, M., DE JESUS, J.C., STEINFELD, A. (2006). "Hydrogen production by steam-gasification of petroleum coke using concentrated solar power—II Reactor design, testing, and modeling", *Int. J. of Hydrogen Energy* **31**(6), 797-811.

Z'GRAGGEN, A. (2008). "Solar Gasification of Carbonaceous Materials - Reactor Design. Modeling, and Experimentation", PhD thesis, ETH-Zurich.